

FIRST INTERFEROMETRIC OBSERVATIONS OF MOLECULAR GAS IN A POLAR RING: THE HELIX GALAXY NGC 2685

EVA SCHINNERER¹ AND NICK SCOVILLE²
Radio Astronomy, MS 105-24, California Institute of Technology, Pasadena, CA 91125-2400

ABSTRACT

We have detected four Giant Molecular cloud Associations (GMAs) (sizes $\leq 6.6'' \approx 430 pc$) in the western and eastern region of the polar ring in NGC 2685 (the Helix galaxy) using the Owens Valley Radio Observatory (OVRO) millimeter interferometer. Emission from molecular gas is found close to the brightest H α and HI peaks in the polar ring and is confirmed by new IRAM 30m single dish observations. The CO and HI line velocities are very similar, providing additional kinematic confirmation that the CO emission emerges from the polar ring. For the first time, the total molecular mass within a polar ring is determined ($M_{H_2} \sim (8 - 11) \times 10^6 M_\odot$, using the standard Galactic conversion factor). We detect about $M_{H_2} \sim 4.4 \times 10^6 M_\odot$ in the nuclear region with the single dish. Our upper limit derived from the interferometric data is lower ($M_{H_2} \leq 0.7 \times 10^6 M_\odot$) suggesting that the molecular gas is distributed in an extended ($\geq 1.3 kpc$) diffuse disk. These new values are an order of magnitude lower than in previous reports. The total amount of molecular gas and the atomic gas content of the polar ring are consistent with formation due to accretion of a small gas-rich object, such as a dwarf irregular. The properties of the NGC 2685 system suggest that the polar ring and the host galaxy have been in a stable configuration for a considerable time (few Gyr). The second (outer) HI ring within the disk of NGC 2685 is very likely at the outer Lindblad resonance (OLR) of the $\sim 11 kpc$ long stellar bar.

Subject headings: galaxies: ISM – galaxies: kinematics and dynamics – galaxies: individual(NGC 2685)

1. INTRODUCTION

Polar ring galaxies (PRGs) represent an unusual, rare class of objects which show clear signs of galaxy interaction (Schweizer, Whitmore & Rubin 1983). Typically, an early-type (S0 or E) host galaxy is surrounded by a luminous ring (containing stars, gas and dust) of ~ 5 to 25 kpc diameter oriented almost perpendicular to the main stellar disk and rotating about the center of the main stellar body (see PRG atlas by Whitmore et al. 1990). To-date only about a dozen PRGs have been kinematically confirmed (e.g. Table 1 in Sparke & Cox 2000). In the generally accepted picture, the formation of polar rings is the result of a "secondary event": e.g., capture of a satellite galaxy or accretion of material between (tidally) interacting galaxies involving a pre-existing S0 galaxy (e.g. Toomre & Toomre 1972, Reshetnikov & Sotnikova 1997). Recently Bekki (1997, 1998) suggested a pole-on merger between two disk galaxies as an alternative formation mechanism. Observations suggest that polar rings are long-lived structures (Whitmore et al. 1987, Eskridge & Pogge 1997). Possible stabilizing mechanisms are self-gravitation in the ring (Sparke 1986), or a massive triaxial halo (Whitmore et al. 1987, Reshetnikov & Combes 1994)

The Helix galaxy, NGC 2685 ($D \sim 13.5 Mpc$; $1'' \sim 65 pc$; (R)SB0+ pec) is one of the kinematically confirmed PRGs. Two rings are detected in HI line emission which have orthogonal angular momentum vectors (Shane 1980). Optical and NIR surface photometry (Peletier & Christodoulou 1993) suggests an age of 2-6 Gyr for the inner 'polar' ring and therefore a long-lived structure. The younger HII regions in the polar ring of NGC 2685 have solar abundances, making accretion of metal-poor material

unlikely (Eskridge & Pogge 1997).

2. OBSERVATIONS

NGC 2685 was observed in its $CO(1-0)$ line with three pointings covering the entire polar ring between 2000 April and June using the six-element Owens Valley Radio Observatory (OVRO) millimeter interferometer in its C and L configurations. The resulting baselines (15 - 115 m) provide a spatial resolution of $\sim 6.6''$ (430 pc) with natural weighting. The noise per $10 km s^{-1}$ channel is $\sim 16 mJy beam^{-1}$ in the combined data of 6 tracks. For the intensity map only emission above the clipping level of 2.5σ was added together.

The IRAM 30m telescope was pointed towards six positions in NGC 2685 based on the OVRO data (indicated in Fig. 1). Position N and W1 were observed on 2002 March 11 (the remaining ones on May 25) in the $CO(1-0)$ and $CO(2-1)$ line using the two 3mm receivers (HPBW $\sim 21''$) and one 1mm receiver (HPBW $\sim 11''$). The observations had a total on-source integration time of about 20 min (W2) to 65 min (N) with an average of 35 min per position. The 1 MHz filter banks provided a velocity resolution of $\sim 2.6 km s^{-1}$ ($\sim 1.6 km s^{-1}$) per channel for the $CO(1-0)$ ($CO(2-1)$) line. The final r.m.s. in a smoothed $10 km s^{-1}$ wide channel was about 4 mK at 115 GHz and 6 mK at 230 GHz.

We also used archival 21cm HI Very Large Array (VLA) data which are described in Mahon (1992). The spatial resolution of the combined data (BnC and D configurations) is $34.6'' \times 33.7''$ ($12.7'' \times 10.8''$) for natural (uniform) weighting with a channel width of $20.7 km s^{-1}$ and an r.m.s. of $1\sigma \approx 0.3(0.5) mJy beam^{-1}$ for natural (uni-

¹ es@astro.caltech.edu

² nzs@astro.caltech.edu

form) weighting.

3. DISTRIBUTION AND KINEMATICS OF THE ATOMIC AND MOLECULAR GAS

3.1. Atomic Gas

The atomic gas forms two distinct rings with radii of $\sim 2.4'$ and $\sim 0.57'$ which can be easily kinematically distinguished in the VLA channel maps (Fig. 3.3 of Mahon 1992). We calculated separate data cubes which contain only emission from the inner and outer ring by blanking the according component in the individual channel maps (Fig. 2). The velocity field of each component is well ordered and shows the spider diagram typical of an inclined rotating disk. We used tilted-ring fitting routines to derive the kinematic parameters (inclination, position angle, dynamical center, systemic velocity) and the HI rotation curve. The position angle ($PA = 35^\circ \pm 1^\circ$) of the kinematic major axis of the outer HI ring is aligned with the major axis of the S0 host disk ($PA \sim 37^\circ$; Fig. 3). The position angle of the inner polar ring is off-set by about 70° . However, the inclination derived for the two HI gas rings and the inner S0 host are similar ($i \sim 65^\circ$) within the errors (see also Shane 1980, Mahon 1992). For the final rotation curve, we assumed that the rotation velocities in the polar ring reflect those in the HI disk at the corresponding radii (Fig. 3). The rotation curve is consistent with solid body rotation out to a radius of $\sim 50''$ (3.3 kpc) which includes the position of the polar ring ($r \sim 0.57' \approx 2.2 \text{ kpc}$).

Outer HI ring: The outer HI ring is situated at a radius of $r \sim 2.4'$ ($\approx 9.4 \text{ kpc}$) in a large-scale ($r \sim 2.6' \approx 10.1 \text{ kpc}$) diffuse disk. The HI column density exceeds $\sim 1 \times 10^{21} \text{ cm}^{-2}$ in a few locations within the outer ring at scales of $\sim 10''$. The outer ring contains an atomic gas mass of about $8.8 \times 10^8 M_\odot$ or about 62% of the total atomic gas mass ($1.41 \times 10^9 M_\odot$). In the DSS2 red image a very faint ring-like structure surrounding the main stellar disk (see also Peletier & Christodoulou 1993) coincides with the HI ring (Fig. 3). The change in position angle and ellipticity at $r \sim (80 - 90)''$ are indicative of a bar with a similar semi-major axis length (Fig. 3). If we assume the standard relation between the corotation resonance (CR) radius and the bar semi-major axis a ($r_{CR} = 1.2a$), we find $r_{CR} \approx 100''$ and a bar pattern speed of $\Omega \sim 25 - 30 \text{ km s}^{-1} \text{ kpc}^{-1}$. The position of the outer Lindblad resonance (OLR) lies approximately at the radius of the HI ring under these assumptions (Fig. 3).

Polar HI ring: The H α image by Eskridge & Pogge (1997) shows about 20 HII regions which delineate the polar ring (Fig. 1). The HI polar ring coincides with the H α and optical-continuum emission forming the polar ring (Fig. 2 and Fig. 1). The polar HI ring contains about $2.9 \times 10^8 M_\odot$ or 20% of the total atomic gas mass. This is about 4% of the dynamical mass at this radius ($M_{dyn}(r = 34'') = 7.4 \times 10^9 M_\odot$; assuming spherical symmetry). The average HI column density in the western part of the polar ring is about $1.4 \times 10^{21} \text{ cm}^{-2}$ (peak of $2.1 \times 10^{21} \text{ cm}^{-2}$). In the eastern part, the average HI column density is just below 10^{21} cm^{-2} on scales of $\sim 10''$.

3.2. The Molecular Gas

$CO(1 - 0)$ line emission is detected with the OVRO mm-interferometer in the eastern and western edge of the

polar ring of NGC 2685 (Fig. 1). The CO data are summarized in Table 1. No molecular line emission above 3σ is seen from the nuclear region, even when smoothed to a spectral resolution of 130 km s^{-1} ($1\sigma \approx 6 \text{ mJy/beam}$). The four GMAs in the polar ring are spatially unresolved at our resolution of $\sim 6.6''$ ($\approx 430 \text{ pc}$). The molecular gas is located close to the densest HI peaks in the polar ring (Fig. 1) which are also next to the brightest H α regions. The velocities and line widths of the molecular gas agree well with those seen in the atomic gas of the polar ring (Fig. 4), providing kinematic confirmation that the CO emission is located in the polar ring and not in the S0 host.

A comparison of the CO line flux detected in the OVRO data with the IRAM 30m single dish line flux in the western (eastern) part of the ring shows that the OVRO data recovers about 90 (40) % of the single dish flux (Table 1). Both ^{12}CO lines are detected in both sides of the polar ring with the IRAM single dish telescope (Fig. 4). The line FWHMs are fairly small (20 km s^{-1} and 15 km s^{-1} for $CO(1 - 0)$ and $CO(2 - 1)$). The properties of the GMAs (size $\leq 430 \text{ pc}$, velocity widths $\sim 15 \text{ km s}^{-1}$) are comparable to those seen in other galaxies (e.g. in M 51, Aalto et al. 1999). Using the upper mass limit of $0.2 \times 10^6 M_\odot$ from position W2 (Table 1), we derive an upper limit for the total undetected molecular gas mass in the polar ring of about $6 \times 10^6 M_\odot$. The central $CO(1 - 0)$ IRAM spectrum clearly shows a 130 km s^{-1} wide line at the $\sim 3\sigma$ level of $\sim 6 \text{ mK}$. Using the relation $S_O/S_I = (1 + (\frac{\theta_S}{\theta_I})^2)/(1 + (\frac{\theta_S}{\theta_O})^2)$ between the ratios of the fluxes ($S_{I,O}$ and the beam ($\theta_{I,O}$) and source sizes (θ_S) (e.g. Dickel 1976) for the IRAM (I) and OVRO (O) data, we find that the extent of the CO emission must be of the order of $\sim 20''$ to explain the OVRO non-detection.

3.3. Comparison to previous CO detections

Our CO line fluxes for the polar ring (region E1 and W1) are considerably smaller than those previously reported by Watson, Guptill & Buchholz (1994) (their position 3 and 7). Given the good agreement between our CO line widths ($\sim 20 \text{ km s}^{-1}$) and the HI line width (compared to the CO line widths of $\sim 130 \text{ km s}^{-1}$ by Watson et al. 1994) together with the consistency of the OVRO and IRAM data, we conclude that the present data yield more accurate fluxes. The strong $CO(1 - 0)$ line emission apparent in the NRO 45m spectrum (Taniguchi et al. 1990) is also inconsistent with our nuclear line flux.

4. DISCUSSION AND IMPLICATIONS

4.1. Probable formation mechanism of the polar ring

The (detected) molecular gas mass of the polar ring is only about 4% of the atomic mass present there ($\log(M_{H_2}/M_{HI}) \approx -1.40$), and the ratio between the blue luminosity and the molecular gas mass is also fairly low ($\log(M_{H_2}/L_B \approx -2.7)$ using $L_B \sim 4.5 \times 10^9 L_\odot$ of Richter, Sackett & Sparke 1994). These values are comparable to those found for low-mass ($\leq 10^{10} M_\odot$) very late-type galaxies (i.e. including dwarf irregulars, Casoli et al. 1998) and S0 galaxies with counter-rotating gas/stars (Bettoni et al. 2001).

The low far-infrared luminosity of $L_{FIR} \sim 4 \times 10^8 L_\odot$ (using the IRAS fluxes and the standard relation for

L_{FIR} ; Sanders & Mirabel 1996) indicates no recent *masive* star formation as observed in starburst galaxies in the NGC 2685 system. This is in agreement with the old age ($\sim 10 Gyr$) of the nuclear stellar population (Sil'chenko 1998). All this implies that there was no considerable gas inflow into the central kiloparsec in the recent past. This appears to contradict the models of the pole-on disk merger (Bekki 1998) and polar encounter with a spiral galaxy (Reshetnikov & Sotnikova 1997), which show an accumulation of a few $10^8 M_{\odot}$ in the central kiloparsec. (Our derived molecular gas mass in the inner kiloparsec is only about $4 \times 10^6 M_{\odot}$.)

The host disk of NGC 2685 exhibits no obvious sign of an interaction besides the more extended diffuse HI emission at the north-eastern edge of the disk (Fig. 2). We can use equation (29) of Lake & Norman (1983) which relates the density of the accreted dwarf to the mean density of the parent galaxy inside the radius of the orbit. For a dynamical mass of $M_{dyn}(r = 34'') = 7.4 \times 10^9 M_{\odot}$ inside the ring radius for the host galaxy, and a total mass of $M_{dwarf} \sim 5 \times M_{HI,ring} \approx 1.5 \times 10^9 M_{\odot}$ (assuming a typical scale factor of 5 between the HI mass and the dynamical mass for dwarf galaxies; e.g. Swaters 1999), we find a radius for the accreted dwarf galaxy of about 2.2 kpc. This radius and the HI mass of $M_{HI} \sim 3 \times 10^8 M_{\odot}$ are typical values for late-type dwarf galaxies (Mateo 1998, Swaters 1999). Since the ring appears in its colors neither very young ($< 1 Gyr$) nor extremely ancient (Peletier & Christodoulou 1993), it seems likely that the polar ring was formed a few Gyr ago during an accretion event (of a dwarf/low-mass galaxy) similar to those proposed for S0 counter-rotators. The solar metallicity derived for the ring HII regions (Eskridge & Pogge 1997) implies that either (1) the accreted dwarf galaxy had an elevated intrinsic metallicity similar to those observed in a couple local dwarf galaxies (e.g. Mateo 1998), (2) low-level continuous star formation has enriched the polar ring ISM in the past few Gyr (see e.g. Legrand et al. 2001) and/or (3) the ISM of the accreted dwarf galaxy was mixed/enriched with more metal-rich material from the primary galaxy.

The outer HI ring can be explained as gas accumulated

at the OLR of the 11 kpc diameter bar. The good spatial correspondence of the optical and HI rings suggests that there is enhanced star formation. We conclude that the suggested scenario by Peletier & Christodoulou (1993) seems unlikely, where the outer HI ring has been formed during the secondary accretion event which formed the inner polar ring as well.

4.2. Stability of the polar ring

The OVRO map of the molecular gas provides the first unambiguous (kinematically confirmed) detection of molecular gas in a polar ring. This molecular gas is associated with about four GMAs which are located close to on-going star formation and peaks in the atomic gas which exceed $10^{21} cm^{-2}$. Note that the molecular and the atomic gas appear concentrated where the polar ring intersects the disk of the parent galaxy.

The polar ring exhibits at least two stellar populations. The HII regions present in the polar ring have an average age of 5 Myr (if instantaneous star formation is assumed) and about solar metallicity (Eskridge & Pogge 1997). However, Peletier & Christodoulou (1993) deduced an age of a few Gyr from the red colors of the polar ring. The contribution of the atomic gas in the polar ring to the total dynamical mass (enclosed out to its radius) is about 4%. This might already be enough to allow for self-gravitation of the polar ring, and explain its persistence (Sparke 1986). Alternatively, Mahon (1992) has found that the HI distribution and kinematics of NGC 2685 can be stable using models of prograde anomalous orbits in a triaxial gravitational potential.

Thus we conclude that: (a) the polar ring has been stable for a substantial time (few Gyr) and (b) the recent star formation in the polar ring has been triggered by another mechanism than the actual polar ring formation process.

Special thanks to C. Thum for taking the IRAM data and to F. Schweizer for his critical comments on an early draft. We like to thank P. Eskridge for providing us with the $H\alpha$ image. ES acknowledges support by National Science Foundation grant AST 96-13717.

REFERENCES

- Aalto, S., Hüttemeister, S., Scoville, N. Z., & Thaddeus, P. 1999, ApJ, 522, 165
 Bekki, K. 1997, ApJ, 490, L37
 Bekki, K. 1998, ApJ, 499, 635
 Bettoni, D., Galletta, G., García-Burillo, S., & Rodríguez-Franco, A. 2001, A&A, 374, 421
 Casoli, F. et al. 1998, A&A, 331, 451
 Dickel, J. R. 1976, in Methods of Experimental Physics, Part 12c, ed. M. Marton (New York, San Francisco: Academic), 1
 Eskridge, P. B. & Pogge, R. W. 1997, ApJ, 486, 259
 Lake, G. & Norman, C. 1983, ApJ, 270, 51
 Legrand, F., Tenorio-Tagle, G., Silich, S., Kunth, D., & Cerviño, M. 2001, ApJ, 560, 630
 Mahon, M. E. 1992, Ph.D. Thesis, University of Florida
 Mateo, M. L. 1998, ARA&A, 36, 435
 Peletier, R. F. & Christodoulou, D. M. 1993, AJ, 105, 1378
 Reshetnikov, V. P. & Combes, F. 1994, A&A, 291, 57
 Reshetnikov, V. & Sotnikova, N. 1997, A&A, 325, 933
 Richter, O.-G., Sackett, P. D., & Sparke, L. S. 1994, AJ, 107, 99
 Sanders, D. B. & Mirabel, I. F. 1996, ARA&A, 34, 749
 Schweizer, F., Whitmore, B. C., & Rubin, V. C. 1983, AJ, 88, 909
 Shane, W. W. 1980, A&A, 82, 314
 Sil'chenko, O. K. 1998, A&A, 330, 412
 Sparke, L. S. 1986, MNRAS, 219, 657
 Sparke, L. S. & Cox, A. L. 2000, ASP Conf. Ser. 197, 119
 Strong, A. W., et al. 1987, Proc. 20th Intern. Cosmic Ray Conf., I, 125
 Swaters, R. A. 1999, Ph.D. Thesis, Rijksuniversiteit Groningen
 Taniguchi, Y., Sofue, Y., Wakamatsu, K., & Nakai, N. 1990, AJ, 100, 1086
 Toomre, A. & Toomre, J. 1972, ApJ, 178, 623
 Watson, D. M., Guptill, M. T., & Buchholz, L. M. 1994, ApJ, 420, L21
 Whitmore, B. C., Lucas, R. A., McElroy, D. B., Steiman-Cameron, T. Y., Sackett, P. D., & Olling, R. P. 1990, AJ, 100, 1489
 Whitmore, B. C., McElroy, D. B., & Schweizer, F. 1987, ApJ, 314, 439

TABLE 1
SUMMARY OF CO (1-0) DATA

Instrument Component	IRAM						OVRO						
	N	W1	W2	E1	E2	E3	N	W_N	W_S	W_{tot}	E_N	E_S	E_{tot}
I_{CO} [$K km s^{-1}$]	1.01	1.47	≤ 0.46	1.13	1.10	1.18	≤ 1.66	5.13	6.79	13.8	1.17	3.43	4.74
S_{CO} [$Jy km s^{-1}$]	4.82	7.02	≤ 2.20	5.38	5.26	5.62	≤ 0.78	2.41	3.20	6.50	0.55	1.61	2.23
N_{H_2} [$10^{21} cm^{-2}$]	0.20	0.29	≤ 0.01		0.23		≤ 0.33	1.03	1.36	2.76	0.23	0.69	0.95
M_{H_2} [$10^6 M_\odot$]	4.4	6.5	≤ 0.2		5.0		≤ 0.7	2.2	3.0	6.0	0.5	1.5	2.1

Note. — Properties of the molecular gas in NGC 2685 as derived from the single dish and interferometric data. (The uncertainties in the flux measurements are about 10% (15%) for the IRAM (OVRO) data.) The total mapped molecular gas mass in the ring is $8.0 \times 10^6 M_\odot$ compared to $\sim 10^7 M_\odot$ detected by the IRAM single dish. The OVRO upper limit for the nucleus is derived via $S_{CO} = 3\sigma \times \Delta v$ with $\Delta v = 130 km s^{-1}$ from the 30m spectrum. Assuming that the average polar ring GMA has a small line width of $\sim 20 km s^{-1}$, our upper mass limit is $0.4 \times 10^6 M_\odot$ from the OVRO data. We use a standard conversion factor of $X = 2 \times 10^{20} cm^{-2} / (K km s^{-1})$ (Strong et al. 1987).

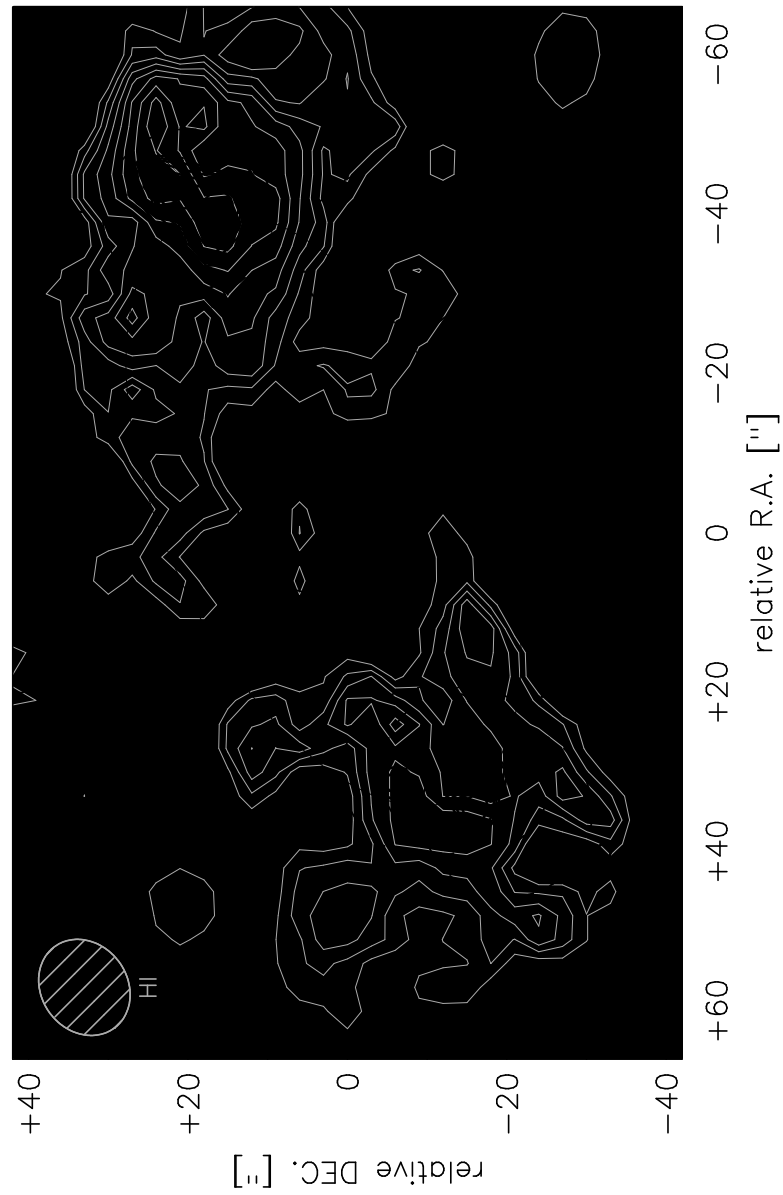


FIG. 1.— The molecular gas as seen in its CO line emission by OVRO (fat black contours) is located close to the densest HI peaks (grey contours) and the HII regions seen in the $H\alpha$ line emission (grayscale). The IRAM 30m pointings are indicated by the broken circles delineating the 3mm HPBW. The thin ellipse indicates the geometry of the polar ring. The beam of the OVRO and HI data are shown.

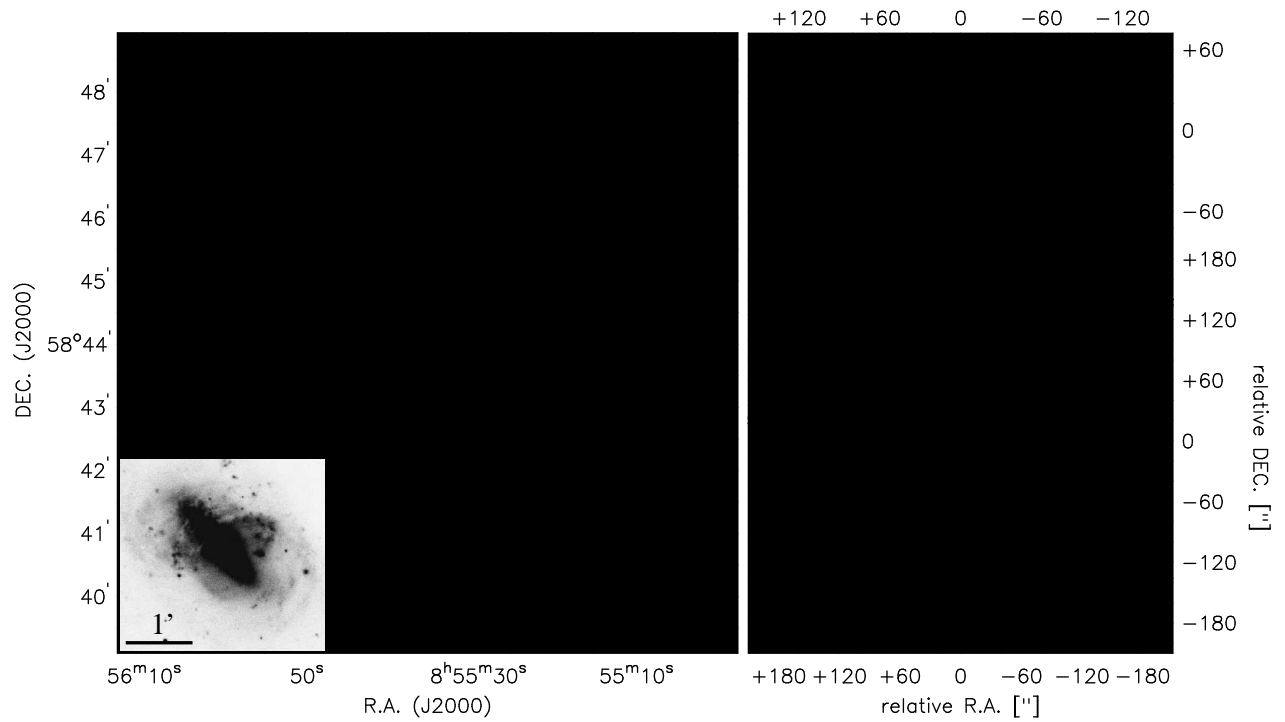


FIG. 2.— Intensity maps (grayscale) and velocity fields (contours) of the VLA HI data. Increasing (solid line) (decreasing; broken line) velocities are shown in steps of 20 km s^{-1} relative to $v_{helio} = 875 \text{ km s}^{-1}$ (thick line). (a) Total HI emission. The inset shows an optical image (from NOAO/AURA/NSF) of NGC 2685. (b) The polar ring component only. (c) The outer HI disk/ring.

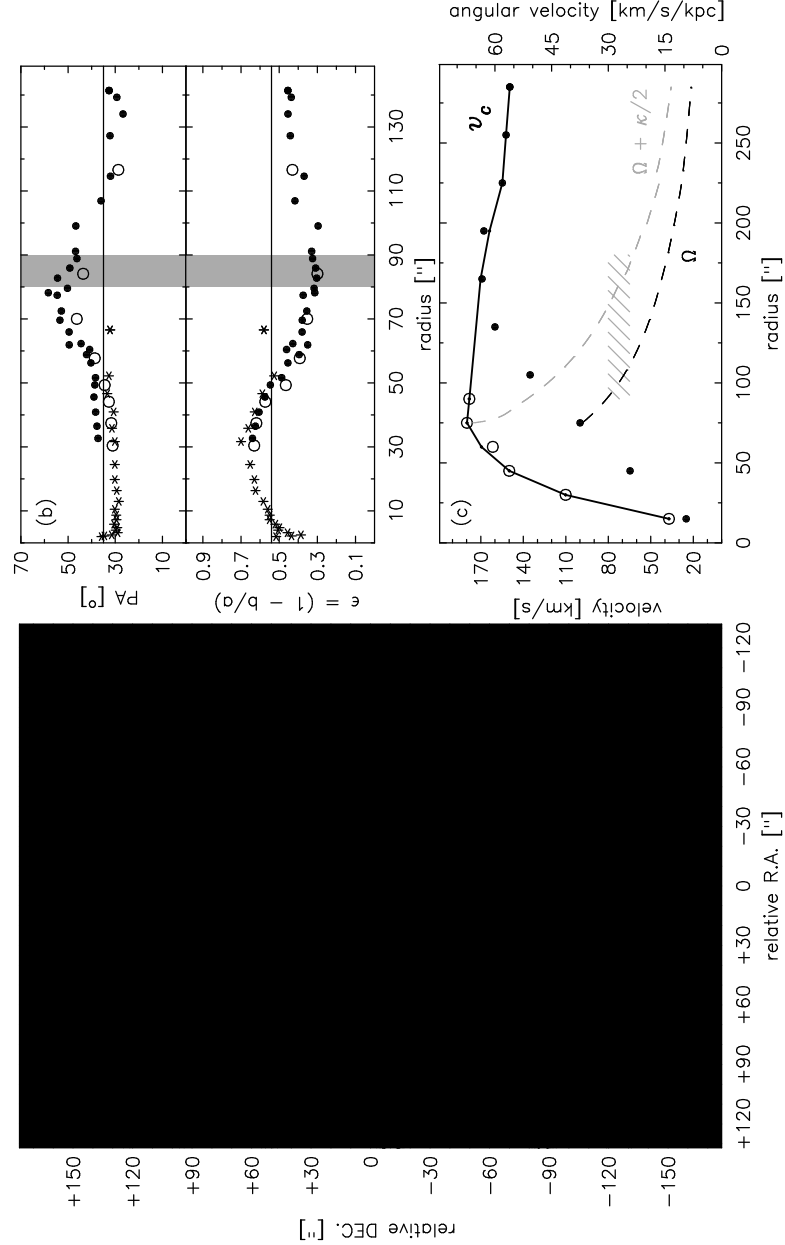


FIG. 3.— (a) Smoothed DSS2 red image (contours) overlaid on the HI outer disk/ring component (see text). (b) The change in ellipticity $\epsilon = (1 - \frac{b}{a})$ and position angle of fitted ellipses to the DSS2 red image (solid circles) indicate a bar semi-major axis of $\sim 80''$ (shaded area). The values of Peletier & Christodoulou (1993) derived from a K band image (stars) and a deep F band image (open circles) are shown as well. (c) The rotation curve derived from the HI data (solid line) and the fits to the natural weighted outer disk only (solid circles) and the polar ring (open circles). The corresponding curves for Ω (broken dark gray line) and $\Omega + \frac{\kappa}{2}$ (broken light gray line) indicate that the OLR is at about $150''$ (hatched area) for a bar semi-major axis length of about $80''$.

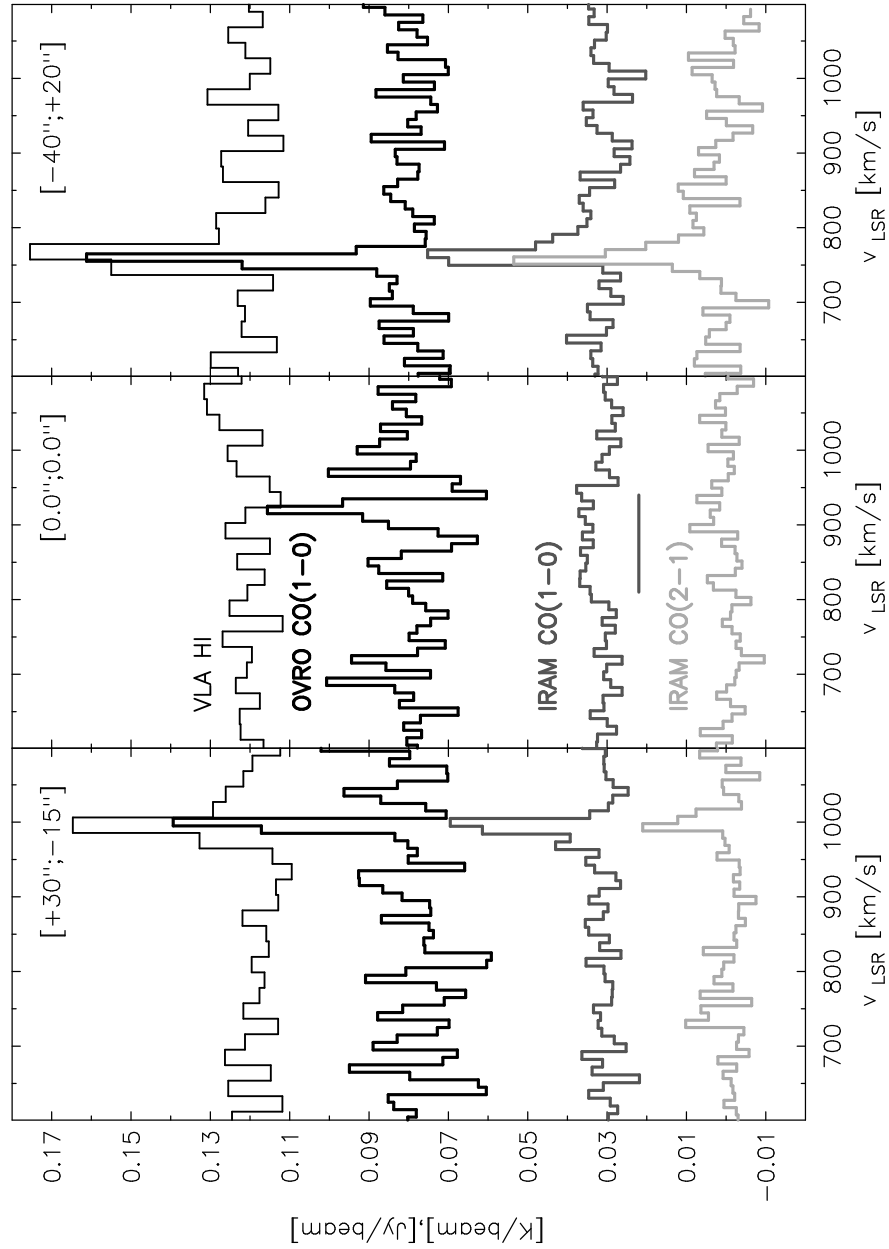


FIG. 4.— Comparison of the HI (thin black line) and CO spectra from the eastern (*left*) and western (*right*) part of the polar ring as well as the nucleus (*middle*). Units are: HI ($[Jy/beam] \times 9$, thin black line), OVRO ^{12}CO ($[Jy/beam]$, thick black line), and IRAM $CO(1-0)$ (thick dark grey line) and $CO(2-1)$ (thick light grey line) in T_A^* ($[K/beam]$). The nuclear IRAM $CO(1-0)$ spectrum shows a wide ($\sim 130 \text{ km s}^{-1}$) line (indicated by the bar) close to the 3σ level.